Acta Crystallographica Section F
Structural Biology and Crystallization Communications
ISSN 1744-3091

Expression, purification, crystallization and structure determination of two glutathione *S*-transferase-like proteins from *Shewanella oneidensis*

Bert Remmerie, Karen Vandenbroucke,‡ Lina De Smet, Wesley Carpentier,§ Dirk De Vos,¶ Jan Stout, Jozef Van Beeumen and Savvas N. Savvides*

Laboratory for Protein Biochemistry and Biomolecular Engineering (L-ProBE), K. L. Ledeganckstraat, Ghent University, B-9000 Ghent, Belgium

‡ Current address: Innogenetics NV, Technology Park 6, 9052 Ghent, Belgium.
§ Current address: Laboratory for Industrial Microbiology and Biocatalysis, Ghent University, Coupure Links 653, 9000 Ghent, Belgium.
¶ Current address: Department of Molecular Cell Physiology, Vrije Universiteit Amsterdam, De Boelelaan 1085, NL 1081 HV Amsterdam, The Netherlands.

Correspondence e-mail: savvas.savvides@ugent.be

Received 2 April 2008
Accepted 14 May 2008

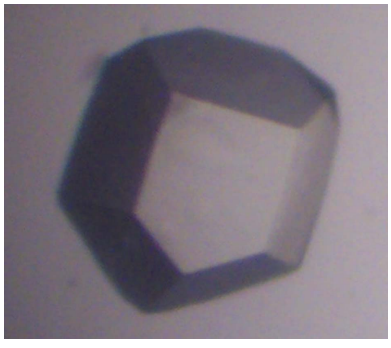

Genome analysis of *Shewanella oneidensis*, a Gram-negative bacterium with an unusual repertoire of respiratory and redox capabilities, revealed the presence of six glutathione *S*-transferase-like genes (*sogst1–sogst6*). Glutathione *S*-transferases (GSTs; EC 2.5.1.18) are found in all kingdoms of life and are involved in phase II detoxification processes by catalyzing the nucleophilic attack of reduced glutathione on diverse electrophilic substrates, thereby decreasing their reactivity. Structure–function studies of prokaryotic GST-like proteins are surprisingly underrepresented in the scientific literature when compared with eukaryotic GSTs. Here, the production and purification of recombinant SoGST3 (SO_1576) and SoGST6 (SO_4697), two of the six GST-like proteins in *S. oneidensis*, are reported and preliminary crystallographic studies of crystals of the recombinant enzymes are presented. SoGST3 was crystallized in two different crystal forms in the presence of GSH and DTT that diffracted to high resolution: a primitive trigonal form in space group $P3_1$ that exhibited merohedral twinning with a high twin fraction and a primitive monoclinic form in space group $P2_1$. SoGST6 yielded primitive orthorhombic crystals in space group $P2_12_12_1$ from which diffraction data could be collected to medium resolution after application of cryo-annealing protocols. Crystal structures of both SoGST3 and SoGST6 have been determined based on marginal search models by maximum-likelihood molecular replacement as implemented in the program *Phaser*.

1. Introduction

Glutathione *S*-transferases (GSTs; EC 2.5.1.18) are a ubiquitous family of enzymes that are found in all kingdoms of life. They are involved in phase II detoxification processes and catalyze the nucleophilic attack of the tripeptide glutathione (γ-glutamyl-cysteinyl-glycine; GSH) on a wide range of endobiotic and xenobiotic electrophilic substrates, thereby decreasing their reactivity towards cellular macromolecules (Armstrong, 1997). In addition to their catalytic role in detoxification, GSTs exhibit binding to diverse ligands (Listowsky *et al.*, 1988; Ketley *et al.*, 1975; Barycki & Colman, 1997) and have been implicated in a variety of resistance phenomena against cancer-chemotherapy agents (Tew, 1994; McLellan & Wolf, 1999), insecticides (Tang & Tu, 1994; Ranson *et al.*, 1997), herbicides (Edwards *et al.*, 2000; Dixon *et al.*, 1998) and antibiotics (Arca *et al.*, 1990). Taken together, these structure–function characteristics have formed the basis for the use of GSTs as enzymatic platforms for the bioremediation of xenobiotic chemicals.

GSTs can be classified into three major subfamilies based on their cellular localization: (i) cytosolic GSTs, (ii) microsomal GSTs and (iii) peroxisomal/mitochondrial GSTs, which are also called κ-class GSTs (Hayes *et al.*, 2005; Morel *et al.*, 2004; Ladner *et al.*, 2004). The latter group of GSTs are structurally very distinct from the cytosolic and microsomal GSTs, which are dimeric and trimeric proteins, respectively (Robinson *et al.*, 2004). The cytosolic class of GSTs has been further organized into an ever-increasing number of divergent subclasses based on amino-acid/nucleotide composition and immunological, kinetic and structural features. Members within a given sub-

Table 1
Crystal data and data-collection statistics.

Values in parentheses are for the highest resolution shell.

	SoGST3-*A*	SoGST3-*B*_1	SoGST3-*B*_2	SoGST6_1 (−GSH)	SoGST6_2 (+GSH)
X-ray source/beamline	ESRF/SNBL	DESY/BW7A	SLS/X06SA	DESY/X11	DESY/X11
Temperature (K)	100	100	100	100	100
Wavelength (Å)	0.8730	0.9795	1.0073	0.8116	0.8126
Frame oscillation (°)	1.0	1.0	0.25	0.5	1.0
Data-processing software	*DENZO*/*SCALEPACK*	*DENZO*/*SCALEPACK*	*XDS*/*XSCALE*	*DENZO*/*SCALEPACK*	*DENZO*/*SCALEPACK*
Space group	$P3_1$	$P2_1$	$P2_1$	$P2_12_12_1$	$P2_12_12_1$
Resolution (Å)	1.8 (1.83–1.8)	2.1 (2.14–2.1)	1.23	2.95 (3.0–2.95)	2.6 (2.66–2.6)
Unit-cell parameters (Å, °)	a = 85.98, b = 85.98, c = 111.53	a = 49.84, b = 122.21, c = 77.47, β = 107.4	a = 49.02, b = 122.42, c = 76.53, β = 107.3	a = 51.51, b = 93.72, c = 99.35	a = 50.92, b = 93.35, c = 99.85
No. of molecules in ASU	2	4	4	2	2
No. of observed reflections	411032	281501	773956	24602	64414
No. of unique reflections	84205	50816	245009	9313	15387
Mosaicity (°)	0.50	0.60	0.25	0.75	0.60
Completeness (%)	98.6 (92.2)	99.4 (90.2)	98.5 (88.4)	86.8 (74.5)	99.9 (99.3)
Redundancy	4.9	5.5	3.1	2.6	4.2
$R_{\rm meas}$† (%)	7.2 (43.5)	9.9 (22.5)	6.3 (54.5)	10.4 (63.4)	11.6 (45.2)
$\langle I/\sigma(I)\rangle$	25.0 (2.5)	15.8 (7.0)	9.7 (2.1)	12 (1.9)	12 (3.6)

† $R_{\rm meas}$ is the multiplicity-weighted $R_{\rm merge}$, *i.e.* $\sum_{hkl}\sum_i[N/(N-1)]^{1/2}|I_i(hkl)-\langle I(hkl)\rangle|/\sum_{hkl}\sum_i I_i(hkl)$, where $I_i(hkl)$ is the intensity of the ith measurement of reflection hkl and $\langle I(hkl)\rangle$ is the average value over multiple measurements (Diederichs & Karplus, 1997).

class of cytosolic GSTs typically share 40–50% sequence identity and only 25–30% when compared with members of other subclasses.

Cytosolic GSTs are dimeric proteins, with each subunit comprising distinct N- and C-terminal domains. The N-terminal domain adopts a topology similar to that of thioredoxin (Wilce & Parker, 1994), while the C-terminal domain is largely α-helical and is delineated from the N-terminal domain *via* a linker sequence. The active site of these GSTs exhibits two binding regions: a conserved hydrophobic G-site where GSH binds and a more variable H-site where hydrophobic electrophilic ligands bind (Armstrong, 1997; Sheehan *et al.*, 2001).

Genome analysis of *Shewanella oneidensis*, a Gram-negative facultative anaerobic bacterium that serves as an important model organism for bioremediation studies owing to its diverse respiratory and redox capabilities, revealed the presence of six glutathione *S*-transferase-like genes (*sogst1*–*sogst6*). Two of these GST gene products, SoGST1 and SoGST6, exhibit high sequence similarities (38% and 46%, respectively) to dichloromethane dehalogenases (DCM dehalogenase; EC 4.5.1.3), suggesting a possible role of *S. oneidensis* in dehalogenation reactions.

Here, we report the successful overexpression, purification, crystallization and structure determination by molecular replacement of recombinant SoGST3 and SoGST6. The availability of crystal structures of these bacterial GSTs will help to broaden the limited pool of structure–function relationships available for prokaryotic GSTs.

2. Materials and methods

2.1. Cloning and protein expression

The genes encoding SoGST3 and SoGST6 were amplified by PCR using the genomic DNA of *S. oneidensis* strain MR-1 as a template and were subcloned into the pGEM-T vector using the TA cloning system. This resulted in plasmid pGEM-*sogstx* (where *x* denotes the corresponding number of the gene). The primers used to amplify the genes included *Nco*I and *Bam*HI restriction sites to facilitate cloning in pET-15b carrying the inducible T7 promotor. The *sogst3* and *sogst6* gene fragments were inserted into the pET-15b vector as *Nco*I–*Bam*HI fragments, resulting in pET-15b/*sogst3* and pET-15b/*sogst6*.

Escherichia coli BL21 (DE3) cells were transformed by electroporation with pET-15b/*sogst3* or pET-15b/*sogst6* plasmid. Precultures of the transformed cells were grown overnight at 310 K in LB broth and were subsequently diluted 100-fold in fresh medium and allowed to grow at 310 K in a rotary shaker operating at 200 rev min^{-1}. Overexpression of *sogst3* and *sogst6* was induced with 1 m*M* IPTG (final concentration) at an OD_{600} of 0.6. After overnight induction, the cells were harvested by centrifugation at 277 K and 1400 rev min^{-1}. The cell pellet was resuspended in 10 m*M* Tris–HCl pH 7 and stored at 193 K. Cells were disrupted by sonication and the soluble protein fraction was clarified by centrifugation at 14 000 rev min^{-1} for 30 min at 277 K.

2.2. Protein purification

SoGST3 was purified to homogeneity using a four-step procedure. The clarified lysate was filtered (0.22 µm) before loading onto a 10 ml Q-Sepharose Fast Flow column connected to an ÄKTA system (GE Healthcare) pre-equilibrated with 50 m*M* Tris–HCl pH 7.4 at room temperature. The column was eluted with a linear NaCl gradient (0–1 *M*); SoGST3 eluted at 170 m*M* NaCl. The SoGST3-containing fractions were pooled and precipitated with 75%(*w*/*v*) ammonium sulfate. The precipated protein was dissolved in a minimal amount of 50 m*M* Tris–HCl pH 7.4 and subsequently desalted on a HiPrep 26/10 column (GE Healthcare). SoGST3-containing fractions were pooled and loaded back onto the 10 ml Q-Sepharose column, which was pre-equilibrated with 50 m*M* MES pH 6.0. SoGST3 eluted at 250 m*M* NaCl using a linear NaCl gradient (0–1 *M*). As a final step, SoGST3 was applied onto a HiLoad 16/60 Superdex 200 prep-grade column pre-equilibrated with 50 m*M* MES pH 6.0, 150 m*M* NaCl. SoGST3 eluted at 80 ml, which corresponds to the mass of a hexamer. The purified protein was concentrated to 11 mg ml^{-1}.

SoGST6 was purified to homogeneity in a three-step purification process. The bacterial lysate was fractionated by ammonium sulfate precipitation and SoGST6 precipitated at 40–50% ammonium sulfate. The precipitated protein was dissolved in PBS buffer and desalted on a HiPrep 26/10 desalting column pre-equilibrated with 10 m*M* sodium citrate pH 6.0. The protein was applied onto an SP-Sepharose column pre-equilibrated with 10 m*M* sodium citrate pH 6.0. Based on the theoretically determined pI of the protein, which was 5.17, we were surprised that the protein showed no affinity for the resin at pH 6. The flowthrough was then loaded onto a Q-Sepharose column connected to an ÄKTA system (GE Healthcare) pre-equilibrated with 10 m*M* sodium citrate pH 6.0. The protein eluted at 130 m*M*

NaCl using a linear gradient of NaCl (0–1 *M*). A persistent contaminant protein of about 55 kDa was removed by a third ion-exchange chromatography step employing a Mono-Q column pre-equilibrated with 50 m*M* Na_2HPO_4 pH 6.3. The protein was brought to 50 m*M* Na_2HPO_4 prior to loading onto the column. Finally, the protein was concentrated to 7 mg ml^{-1} in 20 m*M* MES pH 6.3 using a centrifugal filter device (Millipore) with a 10 kDa cutoff.

Each purification step was analyzed by SDS–PAGE and the concentrations of the proteins were determined by the Bradford method (Bradford, 1976). Protein purity and the presence of GSH covalently bound to the enzymes were assessed by electrospray-ionization mass spectrometry (ESI-MS).

2.3. Protein crystallization

All crystallization experiments were carried out using the hanging-drop vapour-diffusion method by sealing 18 mm siliconized round cover slides carrying droplets containing 1 µl protein solution and 1 µl reservoir solution over 500 µl reservoir solution at 293 K. SoGST3 at 11 mg ml^{-1} in 50 m*M* MES pH 6.0, 150 m*M* NaCl and SoGST6 at 7 mg ml^{-1} in 20 m*M* MES pH 6.3 were screened for crystallization leads against Screens 1 and 2 from Molecular Dimensions Ltd. SoGST6 was further screened against the PEG/Ion Screen (Hampton Research). Promising leads were optimized by additional crystallization grids in which the precipitant concentration was varied against a range of pH values.

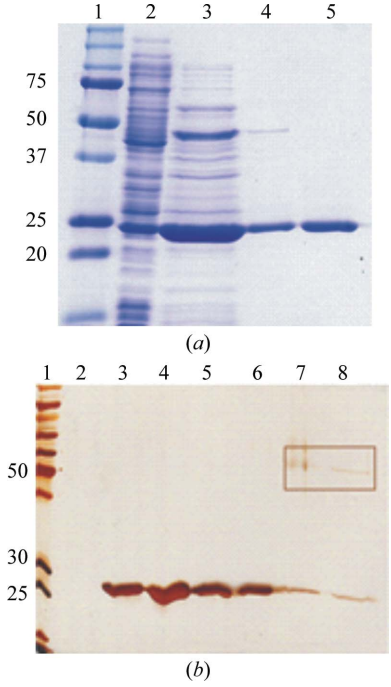

Figure 1
SDS–PAGE analysis of purified SoGST3 and SoGST6. (*a*) Coomassie-stained SDS–PAGE of purified SoGST3. Lane 1, molecular-weight markers (kDa); lane 2, supernatant after sonication of cells expressing recombinant SoGST3; lane 3, SoGST3-containing fraction after anion-exchange chromatography (Q-XL, pH 7.4); lane 4, SoGST3-containing fraction after a second anion-exchange step (Q-XL, pH 6); lane 5, pure enzyme after gel-filtration chromatography. (*b*) Silver-stained SDS–PAGE of purified SoGST6. Lane 1, molecular-weight markers (kDa); lanes 3–6, fractions of the elution peaks from the Mono-Q ion-exchange column (eluting at 170 m*M* NaCl) containing pure SoGST6; lanes 7 and 8, fractions containing the endogenous *E. coli* contaminant (indicated with a frame) eluting at 295 m*M* NaCl.

2.4. Crystal handling, data collection, processing and analysis

Crystals of SoGST3 and SoGST6 were first mounted in quartz capillaries directly from their crystallization drops and their diffraction quality was tested using our in-house X-ray source (a DIP2030 detector mounted on a Bruker–Nonius FR591 rotating-anode generator operating at 45 kV and 90 mA and producing Cu $K\alpha$ X-rays focused with Osmic mirrors to a wavelength of 1.54 Å).

To prepare crystals for data collection under cryogenic conditions (100 K), candidate crystals were transferred to crystal-stabilizing solutions supplemented with either 30%(*v*/*v*) PEG 400 or 25%(*v*/*v*) glycerol and flash-cooled in cryo-loops of appropriate size (Hampton Research) by plunging them directly into liquid nitrogen.

X-ray diffraction data from a single SoGST3 crystal were collected on the Swiss–Norwegian Beamline (SNBL) at the European Synchrotron Radiation Facility (ESRF, Grenoble) at a wavelength of 0.8730 Å using a MAR CCD (MAR Research) detector system. Owing to the presence of several reflections with intensities that exceeded the dynamic range of the detector, the data-collection strategy was split into high- and low-resolution passes. A total of 120 rotation images were recorded for the high-resolution pass, with a crystal oscillation angle of 1° and a crystal-to-detector-distance of

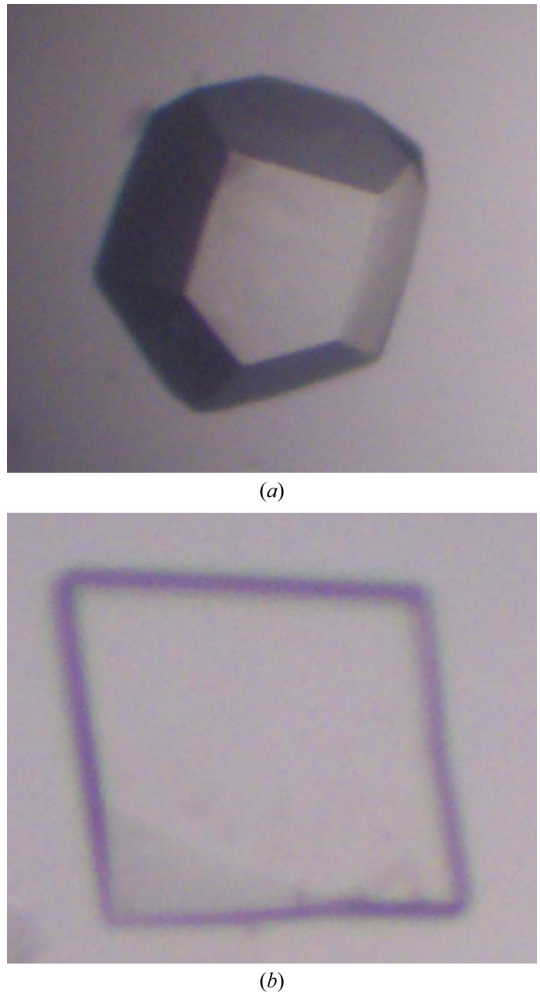

Figure 2
Crystals of SoGST3. (*a*) Representative crystal of the primitive trigonal form (SoGST3-*A*; Table 1) obtained from 22%(*w*/*v*) PEG 4000, 0.1 *M* CHES pH 9, 0.25 *M* calcium chloride, 4 m*M* GSH. (*b*) The primitive monoclinic crystal form (SoGST3-*B*; Table 1) grown from 22%(*w*/*v*) PEG 4000, 0.1 *M* CHES pH 9, 0.25 *M* calcium chloride, 2 m*M* GSH and 0.5 m*M* DTT.

200 mm. The crystal-to-detector-distance was then adjusted to 300 mm for the low-resolution pass and a total of 120 rotation images were recorded with an oscillation angle of 1°.

Data sets from single SoGST3 crystals grown from the same condition but with different morphologies were collected on beamline BW7A of the EMBL Hamburg Outstation at the Deutsches Elektronen-Synchrotron (DESY) operating at a wavelength of 0.9795 Å using a MAR CCD (MAR Research) detector (360 images at 1° oscillations) and on beamline X06SA of the Swiss Light Source (Paul Scherrer Institut, Villigen) operating at a wavelength of 1.0073 Å using a PILATUS 6M counting pixel detector system (1440 images with 0.25° oscillations) (Table 1).

X-ray diffraction data from two single SoGST6 crystals were collected on beamline X11 of the EMBL Hamburg Outstation at the Deutsches Elektronen-Synchrotron (DESY) using a MAR CCD (MAR Research) detector system. A total of 120 rotation images were recorded at a wavelength of 0.8116 Å, with an oscillation range of 0.5° and a crystal-to-detector-distance of 500 mm. A total of 105 rotation images were recorded from a second SoGST6 crystal at a wavelength of 0.8126 Å, with an oscillation range of 1° and a crystal-to-detector-distance of 250 mm.

Data processing was carried out using either the programs *DENZO* and *SCALEPACK* (Otwinowski & Minor, 1997) or *XDS* and *XSCALE* (Kabsch, 1993) (Table 1). Structure determination was carried out by molecular replacement using maximum-likelihood methods implemented in the program *Phaser* v.1.2 (McCoy *et al.*, 2007).

3. Results and discussion

Recombinant SoGST3 and SoGST6 were successfully overexpressed in *E. coli* and purified to homogeneity to milligram amounts (2–5 mg pure protein per litre of culture; Fig. 1). Electrospray-ionization mass spectrometry of purified SoGST3 and SoGST6 revealed molecular weights of 25.49 and 25.69 kDa, respectively, indicating that no GSH molecules were covalently bound to the proteins. This is in contrast to observations for other bacterial GSTs (Rossjohn *et al.*, 1996). This observation is consistent with the fact that the affinity of SoGST3 and SoGST6 for glutathione immobilized on a Sepharose column matrix was too low to allow purification of the enzymes by affinity chromatography. SoGST3 and SoGST6 were instead purified by combining several ion-exchange and gel-filtration chromatographic steps. Interestingly, this low affinity for glutathione-Sepharose has previously been observed for θ-class GSTs, the prototypical class of bacterial GSTs (Vuilleumier, 1997).

Crystallization screens on purified SoGST3 and SoGST6 led to a number of crystallization leads based on polyethylene glycols (PEGs) as precipitating agents, which yielded diffracting crystals upon optimization. SoGST3 crystals grew reproducibly within 4–7 d at 294 K from 20–26%(*w*/*v*) PEG 4000, 1–10 m*M* GSH, 0–0.5 m*M* 1,4-dithiothreitol (DTT), 0.1 *M* CHES pH 9.0, 0.25 *M* calcium chloride. We found that two morphologically different crystal forms of SoGST3 could be grown depending on the relative amounts of GSH and DTT present. One of the crystal forms (SoGST3-*A*) resembled soccer balls (whole or half) and grew to about 0.15 mm on an edge from conditions based on 4–10 m*M* GSH and no DTT (Fig. 2*a*). The second crystal form (SoGST3-*B*) assumed a plate-like shape measuring up to 0.4 × 0.4 × 0.08 mm and typically grew in the presence of 1–2 m*M* GSH and 0.2–0.5 m*M* DTT (Fig. 2*b*). X-ray diffraction data were collected from SoGST3-*A* crystals grown from 22%(*w*/*v*) PEG 4000, 0.1 *M* CHES pH 9, 0.25 *M* calcium chloride, 4 m*M* GSH and from SoGST3-*B* crystals grown from 22%(*w*/*v*) PEG 4000, 0.1 *M* CHES pH 9, 0.25 *M* calcium chloride, 2 m*M* GSH and 0.5 m*M* DTT. Both SoGST3 crystal forms diffracted X-rays to 3–4 Å resolution using our in-house X-ray source and to high resolution using synchrotron radiation (Table 1). Analysis of the crystal-packing densities (Matthews, 1968) for the two crystal forms clearly revealed the

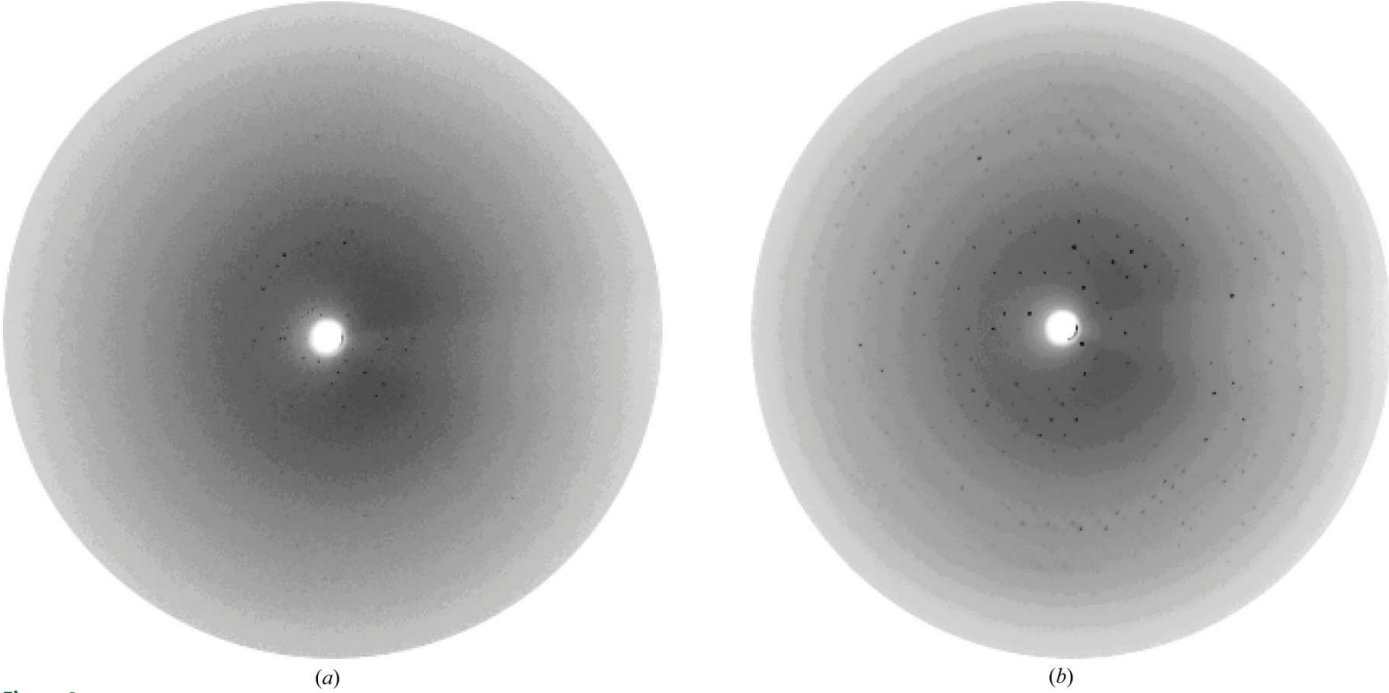

(*a*) (*b*)

Figure 3
Dramatic improvement in the diffraction quality of SoGST6 crystals as result of cryo-annealing. The quality of diffraction images from a SoGST6 crystal at a given crystal-to-detector distance are compared before (*a*) and after (*b*) cryo-annealing. Cryo-annealing was achieved empirically by blocking the stream of nitrogen gas at 100 K using a credit card for 7–10 s followed by cryo-cooling directly in the cryostream without moving the crystal from its mounted position.

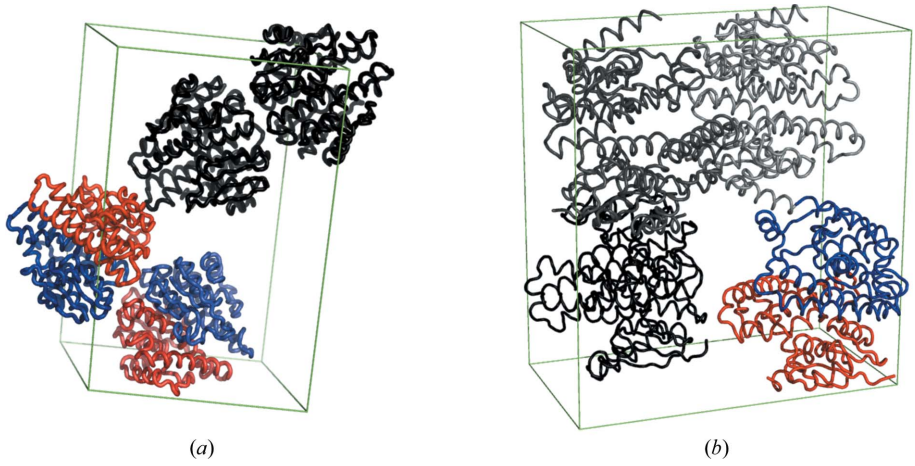

Figure 4
C^{α}-atom traces and packing of SoGST3 (*a*) and SoGST6 (*b*) in their primitive monoclinic and primitive orthorhombic unit cells, respectively. Subunits in dimers making up the asymmetric unit of each lattice are coloured blue and red, while symmetry-related molecules are shown in greyscale. This figure was prepared with the program *PyMOL* (DeLano, 2002).

possibility of one SoGST3 dimer in the primitive trigonal form (SoGST3-*A*) and two SoGST3 dimers in the primitive monoclinic form (SoGST3-*B*).

For SoGST6, needle-like crystals could be optimized to rectangular rod-like crystals measuring 0.1 × 0.1 × 0.3 mm which grew within 3 d at 294 K from 15%(*w*/*v*) PEG 3350, 50 m*M* MES pH 6.3, 0.2 *M* sodium chloride and 0–0.3 m*M* GSH. Data sets were collected from crystals grown in the presence and absence of GSH (Table 1). Initial diffraction images of SoGST6 under cryogenic conditions (100 K) barely extended to 6 Å and exhibited high mosaicity and features of anisotropic diffraction. The diffraction quality could be dramatically improved by cryo-annealing techniques, in which the cryo-stream was blocked for 7–10 s followed by immediate cryocooling of the crystals at 100 K (Heras & Martin, 2005; Fig. 3). The structures of SoGST3 and SoGST6 were determined by molecular replacement using maximum-likelihood methods implemented in the program *Phaser* v.1.2 (McCoy *et al.*, 2007).

Sequence comparison of SoGST3 with structurally characterized GSTs from different cytosolic GST classes revealed that the protein resembles Ure2p from *Saccharomyces cerevisiae*, a θ-class GST (Rossjohn *et al.*, 1996), with a sequence identity of 38%. Higher levels of sequence similarity were observed with respect to uncharacterized GST-like sequences from *Vibrio cholera* (77%) and *Pseudomonas aeruginosa* (72%). A search model for molecular replacement was constructed using Ure2p (Bousset *et al.*, 2001; PDB code 1k0d) in which all nonconserved residues were mutated to alanine and insertions and bound ligands were removed. This resulted in a rather limited search model consisting of one chain of Ure2p containing about 38% of the scattering mass of the target protein. Using a combined rotational and translational search against the 1.80 Å data set from the primitive trigonal crystal form (SoGST3-*A*), two copies of the Ure2p monomer could be positioned in the asymmetric unit with good packing and rather high *Z* scores for the rotation function (RFZ = 4.2) and the translation function (TFZ = 13.9) and a high value for the log-likelihood gain (LLG = 192). The correctness of the molecular-replacement solution was additionally confirmed by the fact that the two positioned monomers in the asymmetric unit of the $P3_1$ unit cell formed a dimer, consistent with the expected quaternary structure of cytosolic GSTs. Furthermore, inspection of initial electron-density maps with Fourier coefficients $2F_o - F_{c,MR}$, $\alpha_{c,MR}$ revealed unique features such as missing side chains and loop regions that were absent in the search model. Initial rounds of crystallographic refinement using simulated annealing, conjugated-gradient energy minimization and *B*-factor refinement protocols implemented in the program *CNS* v.1.1 (Brünger *et al.*, 1998) failed to lead to *R* factors below 50%. Re-examination of the diffraction data led to the conclusion that this crystal form of SoGST3 suffered from merohedral twinning with a large twin fraction (0.48). The data were detwinned using appropriate protocols implemented in the program *CNS* and were subsequently used in further rounds of refinement. This greatly facilitated progress in refinement, but the model once again failed to refine to *R* factors of lower than 40%. In the meantime, data from the primitive monoclinic crystal form of SoGST3, which did not suffer from crystal twinning, became available (SoGST3-*B*). The partially refined model of SoGST3 was used to obtain a molecular-replacement solution in the primitive monoclinic unit cell. Indeed, a solution could readily be obtained for two dimers of SoGST3 related by a noncrystallographic twofold axis in the asymmetric unit of the crystal (Fig. 4*a*), with excellent scores across the board (RFZ = 17.5, TFZ = 40.7, LLG = 2083). Crystallographic refinement is currently under way to atomic resolution against a 1.23 Å data set that has recently become available.

Structure-based multiple sequence alignments of SoGST6 against structurally characterized GSTs identified *E. coli* GST as the closest homologue, with a sequence identity of barely 20%. Remarkably, a search model based on the *E. coli* GST structure (Nishida *et al.*, 1998; PDB code 1a0f) in which all nonconserved residues were mutated to alanine led to a convincing molecular-replacement solution at 3 Å resolution using data set SoGST6_1 (Table 1) for one dimer in the asymmetric unit of the crystal (Fig. 4*b*) with excellent statistics (RFZ = 43, TFZ = 62, LLG = 71). The solution was confirmed by inspection of electron-density maps calculated with Fourier coefficients $2F_o - F_{c,MR}$, $\alpha_{c,MR}$ after refinement of the structure by rigid-body refinement protocols in *CNS* v. 1.1. Crystallographic refinement to 2.6 Å resolution is currently in progress using data set SoGST6_2 (Table 1).

We gratefully acknowledge beam-time allocation and the technical support provided at the EMBL beamlines BW7A and X11 at DESY (Hamburg, Germany), the Swiss–Norwegian Beamline at the ESRF (Grenoble, France) and beamline X06SA of the SLS (Villigen,

Switzerland). BR is a research fellow of the 'Instituut voor de Aanmoediging van Innovatie door Wetenschap en Technologie in Vlaanderen' (IWT). This work was supported in part by a Ghent University GOA grant to JVB and a Ghent University BOF grant to SNS.

References

Arca, P., Hardisson, C. & Suarez, J. E. (1990). *Antimicrob. Agents Chemother.* **34**, 844–848.
Armstrong, R. N. (1997). *Chem. Res. Toxicol.* **10**, 2–18.
Barycki, J. J. & Colman, R. F. (1997). *Arch. Biochem. Biophys.* **345**, 16–31.
Bousset, L., Belrhali, H., Melki, R. & Morera, S. (2001). *Biochemistry*, **40**, 13564–13573.
Bradford, M. M. (1976). *Anal. Biochem.* **72**, 248–254.
Brünger, A. T., Adams, P. D., Clore, G. M., DeLano, W. L., Gros, P., Grosse-Kunstleve, R. W., Jiang, J.-S., Kuszewski, J., Nilges, M., Pannu, N. S., Read, R. J., Rice, L. M., Simonson, T. & Warren, G. L. (1998). *Acta Cryst.* D**54**, 905–921.
DeLano, W. L. (2002). *The PyMOL Molecular Graphics System.* http://www.pymol.org.
Diederichs, K. & Karplus, P. A. (1997). *Nature Struct. Biol.* **4**, 269–275.
Dixon, D. P., Cummins, L., Cole, D. J. & Edwards, R. (1998). *Curr. Opin. Plant Biol.* **1**, 258–266.
Edwards, R., Dixon, D. P. & Walbot, V. (2000). *Trends Plant Sci.* **5**, 193–198.
Hayes, J. D., Flanagan, J. U. & Jowsey, I. R. (2005). *Annu. Rev. Pharmacol. Toxicol.* **45**, 51–88.
Heras, B. & Martin, J. L. (2005). *Acta Cryst.* D**61**, 1173–1180.
Kabsch, W. (1993). *J. Appl. Cryst.* **26**, 795–800.
Ketley, J. N., Habig, W. H. & Jakoby, W. B. (1975). *J. Biol. Chem.* **250**, 8670–8673.
Ladner, J. E., Parsons, J. F., Rife, C. L., Gilliland, G. L. & Armstrong, R. N. (2004). *Biochemistry*, **43**, 352–361.
Listowsky, I., Abramovitz, M., Homma, H. & Niitsu, Y. (1988). *Drug Metab. Rev.* **19**, 305–318.
McCoy, A. J., Grosse-Kunstleve, R. W., Adams, P. D., Winn, M. D., Storoni, L. C. & Read, R. J. (2007). *J. Appl. Cryst.* **40**, 658–674.
McLellan, L. I. & Wolf, C. R. (1999). *Drug Resist. Updat.* **2**, 153–164.
Matthews, B. W. (1968). *J. Mol. Biol.* **33**, 491–497.
Morel, F., Rauch, C., Petit, E., Piton, A., Theret, N., Coles, B. & Guillouzo, A. (2004). *J. Biol. Chem.* **279**, 16246–16253.
Nishida, M., Harada, S., Noguchi, S., Satow, Y., Inoue, H. & Takahashi, K. (1998). *J. Mol. Biol.* **281**, 135–147.
Otwinowski, Z. & Minor, W. (1997). *Methods Enzymol.* **276**, 307–326.
Ranson, H., Prapanthadara, L. & Hemingway, J. (1997). *Biochem. J.* **324**, 97–102.
Robinson, A., Huttley, G. A., Booth, H. S. & Board, P. G. (2004). *Biochem. J.* **379**, 541–552.
Rossjohn, J., Board, P. G., Parker, M. W. & Wilce, M. C. (1996). *Protein Eng.* **9**, 327–332.
Sheehan, D., Meade, G., Foley, V. M. & Dowd, C. A. (2001). *Biochem. J.* **360**, 1–16.
Tang, A. H. & Tu, C. P. (1994). *J. Biol. Chem.* **269**, 27876–27884.
Tew, K. D. (1994). *Cancer Res.* **54**, 4313–4320.
Vuilleumier, S. (1997). *J. Bacteriol.* **179**, 1431–1441.
Wilce, M. C. & Parker, M. W. (1994). *Biochim. Biophys. Acta*, **1205**, 1–18.